The Relative Importance of Wind Strength and Along-Shelf Bathymetric Variations on the Separation of a Coastal Upwelling Jet

RENATO M. CASTELAO AND JOHN A. BARTH

College of Oceanic and Atmospheric Sciences, Oregon State University, Corvallis, Oregon

(Manuscript received 7 March 2005, in final form 7 September 2005)

ABSTRACT

A high-resolution numerical model with idealized topography is used to investigate the degree to which a coastal upwelling jet separates from the shelf as it flows around a submarine bank depending on the wind strength and the horizontal scale of the bank. Experiments were run using several wind forcing magnitudes and submarine banks with different geometries, so as to explore a wide range of the flow strength as measured by the Rossby number (Ro) and the ratio of the squares of the internal Rossby radius of deformation and curvature of the topography as denoted by the Burger number (Bu). The intensity of the jet separation is strongly dependent on both parameters, with maximum separation with increasing Ro and Bu close to 1, when large amounts of upwelled water are exported toward deeper waters. For small Bu, separation is minimal and independent of Ro. For high Ro, the degree of separation decreases at large Bu since the bank acts only as a small perturbation to the flow. Term balances in the along-shelf momentum equation reveal that the primary balance over the bank is between the nonlinear and the ageostrophic terms. In an asymmetric bank, the radius of curvature in the upstream half of the bank dominates in terms of determining the offshore deflection of a water particle at the surface. The asymmetry increases the cross-isobath transport but not the offshore deflection of the jet.

1. Introduction

The response of a stratified coastal ocean to upwelling-favorable winds in regions of uniform along-shelf bottom topography and a straight coastline is relatively well understood. Wind blowing equatorward along the U.S. West Coast, for example, forces an offshore Ekman transport in the surface layer. This results in onshore flow of cold and nutrient-rich waters in the deeper layers. A strong along-shelf southward coastal upwelling jet is formed balanced with the upwelled isopycnals (Huyer 1983). This two-dimensional description anticipates a primary cross-shelf momentum balance between the Coriolis force and the pressure gradient, and the flow is expected to approximately follow the isobaths.

Less is known about the upwelling circulation in regions of along-shelf bottom topography variations. In those regions, the direct coupling between the wind forcing and the along-shelf velocities can be substantially weaker. Kosro (2005), using land-based, high-frequency radar measurements off Oregon from summer 2001, showed that the correlation between meridional currents and meridional wind stress varies spatially. The strongest relation occurs in a region of simple topography, while the relationship breaks down over a shallow submarine bank (Heceta Bank).

In the vicinity of a perturbation in the coastline or bottom topography orientation, the nonlinear advection terms can make a substantial contribution to the momentum balance (Gan and Allen 2002a). In this situation, a gradient wind balance (Holton 1992) is expected to hold, which can be expressed in natural coordinates as

$$\frac{\tilde{v}^2}{r} + f\tilde{v} = -\frac{\partial \Phi}{\partial n}, \tag{1}$$

where r is the local radius of curvature of the trajectory ($r > 0$ for flow turning toward the left following the motion), $\tilde{v}$ is the horizontal speed (a positive definite scalar), f is the Coriolis parameter, Φ is the geopotential field, and n is the directional normal to the flow. The first term is the centripetal acceleration due to the cur-

Corresponding author address: Renato M. Castelao, College of Oceanic and Atmospheric Sciences, Oregon State University, 104 COAS Admin. Bldg., Corvallis, OR 97331-5503.
E-mail: castelao@coas.oregonstate.edu

vature of the trajectory (note that streamlines and trajectories coincide for steady-state motion fields). Yoshida (1967), using a two-layer model, showed that if a cape protrudes into an along-shelf flow, the flow must accelerate locally to get past the cape. As $\tilde{v}$ increases and r become finite (as compared with a straight streamline, where $r \to \infty$), the importance of nonlinear terms increases. Arthur (1965) showed that increased upwelling southward of capes can be partially attributed to variations in relative vorticity, defined in natural coordinates as

$$\zeta = \frac{\tilde{v}}{r} - \frac{\partial \tilde{v}}{\partial n}. \tag{2}$$

Also, if the flow is strong (as to make $\tilde{v}/r$ of the order of f), the centripetal acceleration of the flow itself ($\tilde{v}^2/r$) tends to raise the thermocline near a cape (Clarke 1977). Peffley and O'Brien's (1976) numerical simulations of the three-dimensional upwelling circulation off Oregon suggested that bottom relief can be more important than coastline curvature in causing localized upwelling.

Several studies have been pursued to investigate the behavior of flow around a corner or past an obstacle. The majority of studies exploring a wide range of parameters considered either a homogeneous or a density-driven flow. Bormans and Garrett (1989), for example, used a density-driven flow in a laboratory model to show that for a gyre to form in the lee of a corner, $\tilde{v}/f > R_w$, where R_w is the radius of curvature of the wall. One exception is the work of Boyer and Tao (1987), who used a linearly stratified laboratory model to study flow driven by a body force past a triangular cape in an otherwise flat-bottom channel. They found that the square of the ratio between the Rossby radius of deformation and the size of the cape is an important parameter controlling the generation and propagation of meanders downstream of the cape. Also, Dale and Barth (2001) used an analytic 1.5-layer model of coastal hydraulics with constant potential vorticity in each layer to predict jet separation at Cape Blanco, Oregon. Time-dependent solutions predicted a flow field at critical transitions consisting of a narrow upwelling jet upstream of the cape that moves offshore and broadens at the cape.

The dynamics of upwelling filaments, squirts, and eddies have also been studied, and results suggest that these phenomena originate from the instability of along-shelf currents (McCreary et al. 1991). Haidvogel et al.'s (1991) numerical experiments showed that coastline variability can supply preferred sites for filaments to form. Narimousa and Maxworthy (1989) used a two-layer laboratory model to study the effects of ridges and capes on the generation of standing waves, meanders, filaments, and eddies. The parameter controlling the flow evolution was dependent on the width of the upwelling region at steady state. This may have been affected by their laboratory setup since the offshore migration of the front could artificially increase the cross-shelf pressure gradient owing to the limited size of the tank. A summary of other studies is presented in McCreary et al. (1991).

The dynamics of coastal jet separation is especially interesting, as this feature represents an efficient mechanism for transport of upwelled water to great distances offshore (Brink 1983). Indeed, upwelled water appears to sometimes reach distances offshore greater than the inherent inviscid length scale of the internal Rossby radius of deformation (e.g., Barth et al. 2000). Separation of a coastal jet in an upwelling region has a profound biological implication since it plays a major role in determining to what offshore extent the marine ecosystem can be expected to be stimulated by the nutrient enhancement due to coastal upwelling (Brink 1983). In the present study, a three-dimensional numerical model is used to explore the interactions of a stratified, wind-driven flow with a bottom topographic perturbation over a wide range of parameters, focusing on the jet separation from the topography and consequent shift of the jet core toward deeper waters.

2. Methods

The Princeton Ocean Model (POM) used here is described in detail by Blumberg and Mellor (1987). The model incorporates the Mellor and Yamada (1982) level-2.5 turbulent closure scheme to parameterize vertical mixing. The horizontal diffusion uses the Smagorinsky formulation (Smagorinsky 1963) in which horizontal viscosity coefficients depend on the grid size and velocity gradients. The model domain extends 250 km offshore and 400 km in the along-shelf direction. The grid resolution is 1.5 km in both horizontal directions. In the vertical, 31 sigma levels are utilized with grid spacing that varies so that there is higher resolution near the surface and near the bottom in order to resolve the respective boundary layers. The horizontal velocity $\mathbf{v}$ has components (u, v) corresponding to the cross-shelf and along-shelf velocities in the (x, y) directions so that u is positive onshore and v is positive toward the north. The depth average of the velocity components are denoted by $\mathbf{V}$ and (U, V). We use the notation η for the surface elevation above the undisturbed free surface, T for temperature, and S for salinity.

The idealized bottom topography (Fig. 1) consists of a continental shelf/slope with no variations in the along-

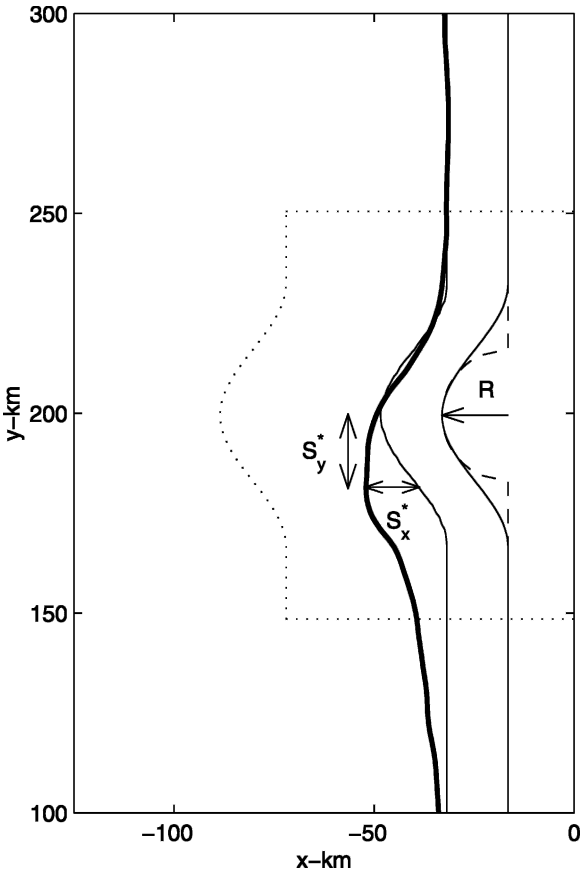

FIG. 1. Idealized bottom topography used in the simulations. Only part of the model domain is shown. Definitions of S_x^*, S_y^*, and R are also shown. The thick line is a transport streamline, and the thin lines are the 100- and 200-m isobaths. The dashed line is a semicircle with radius R. The dotted line denotes the region used to average cross-isobath flow.

shelf direction except where a perturbation in the form of a submarine bank is imposed. The minimum depth is 10 m, and the maximum depth is set to 920 m in order to reduce the constraint on the time steps that are 5 and 150 s for the barotropic and baroclinic modes, respectively. The Coriolis parameter $f = 1.01 \times 10^{-4}$ s^{-1} is constant. The model is initialized with zero velocities and with horizontally uniform stratification. The stratification (obtained from in situ observations) and the bottom slope are representative of the Oregon coastal ocean.

The along-shelf boundary conditions are periodic for all variables. Recently, periodic boundary conditions were employed with success for modeling coastal flows (Gan and Allen 2002a,b; Oke et al. 2002a,b), and they have the advantage of avoiding any questions of artificial along-shelf pressure gradient set up by imperfect open boundary conditions (Gan and Allen 2002a). At the offshore boundary, $\eta_x = V_x = v_x = 0$ (subscripts denote differentiation), and we use a "modified" Orlanski (Camerlengo and O'Brien 1980) radiation conditions for the normal velocities U and u. For T and S, an upstream advection condition is used. The horizontal diffusion coefficient is increased smoothly over eight grid cells adjacent to the offshore boundary to a maximum of 1000 m^2 s^{-1} at the boundary in order to damp out unwanted reflection.

With the objective of minimizing the span of the parameter space, the model was forced by spatially uniform winds in all numerical experiments. The wind forcing was constant in time after being ramped up during one inertial period. Several magnitudes of wind forcing were considered in order to explore how the inertia of the jet affects the flow–topography interaction. The inertia of the jet was measured by averaging the local Rossby number based on surface (upper sigma layer) velocities, given by

$$\mathrm{Ro} = \frac{|\partial v/\partial x - \partial u/\partial y|}{f}, \tag{3}$$

in a region upstream of the bank, extending 60 km in the along-shelf and 120 km in the cross-shelf direction. A large offshore extent was needed in order to encompass the area of increased surface relative vorticity generated by instability of the wind-driven coastal upwelling jet. Similar results are obtained if the Rossby number is computed using the maximum velocity and the jet width as the velocity and length scales, respectively.

The importance of the bank geometry in driving flow separation was explored by using bottom topographies with different radii of curvature R (Fig. 1). The bank extends from midshelf (~40 m) all the way to the bottom of the slope (920 m); that is, there is no coastline perturbation. The radius of curvature is constant (except in a small area up- and downstream of the bank, where the transition to the straight topography region occurs smoothly), although a bank with two different radii is also used in order to represent a geometric asymmetry in the bank (section 6). A Burger number

$$\mathrm{Bu} = \frac{N^2H^2}{f^2R^2} \tag{4}$$

is used to characterize each bottom topography. In (4), $N = [(-g/\rho_0)\partial\rho/\partial z]^{1/2}$ is the buoyancy frequency, ρ is the density, ρ_0 is a constant reference density, H is the undisturbed water depth, and z is the vertical coordinate. The Burger number is formed by the ratio of the squares of the internal Rossby radius of deformation and the radius of curvature of the topography. The internal Rossby radius of deformation was found by solving the vertical mode problem (Kundu et

al. 1975) at the depth occupied by the jet core upstream of the bank for each simulation.

To obtain a quantification of the coastal jet separation, the offshore displacement experienced by a transport streamline in the vicinity of the bank is measured. We first choose a streamline that is located along the core of the jet upstream of the bank. The offshore jet displacement (S_x^*) was determined by differencing the maximum offshore distance reached by the streamline and the offshore distance of the isobath that the streamline occupies upstream of the bank (Fig. 1). The downstream distance from midbank, where the maximum offshore extent reached by the streamline takes place (S_y^*, Fig. 1), was also measured. These two quantities, after being nondimensionalized by the internal Rossby radius of deformation, become S_x and S_y, respectively. A third measure of the coastal jet separation was obtained by determining the depth-averaged cross-isobath flow and computing its spatial average in the vicinity of the bank (D_a). The area where the average is computed extends $3R$ to the north and south of the topography perturbation and from the coast to the 920-m isobath (Fig. 1).

3. Flow response to steady upwelling-favorable winds

Before exploring the flow dependence on the wind forcing and bank geometry, two of the experiments are briefly described: one in which the coastal jet separates at the bank and another in which the jet closely follows the topographic contours. In both experiments, the upwelling-favorable wind stress, after being brought smoothly from 0 to 0.125 Pa, is kept constant. The only difference between the two experiments is the radius of curvature of the topography. The Burger (Rossby) number is estimated to be 1.10 and 0.38 (0.24 and 0.22) for the smaller (R = 19.5 km) and larger (R = 34.5 km) radius simulation, respectively. The effective internal Rossby radius of deformation (Kundu et al. 1975) is approximately 21 km in both cases.

The general characteristics of the flow response to upwelling-favorable winds at day 21 can be seen in a plot of surface velocity vectors overlain on the surface temperature field (Fig. 2). Cross-shelf sections of alongshelf velocity and potential density at several locations, both upstream and downstream of the bank, are plotted for the simulation with the smaller radius bank (Fig. 3). The results upstream of the bank in both simulations are consistent with the general picture of coastal upwelling, with an offshore-directed component at the surface and an onshore flow component at depth (not shown). This offset in the cross-shelf velocity with depth feeds an upwelling circulation. Cold, dense water is advected onshore and vertically, causing the isopycnals to tilt upward (Fig. 3). This results in a decrease of the surface temperature close to the coast (Fig. 2) (Allen et al. 1995).

In the smaller radius simulation (Fig. 2a), the jet accelerates to get past the bank. This is similar to Yoshida's (1967) result of flow accelerating near a cape where there is horizontal convergence due to the narrowing of the boundary section. Velocities are deflected offshore, resulting in large amounts of cold water being driven offshore of the shelf break at the surface. The 10°C isotherm, which closely follows the 200-m isobath upstream of the bank, can be found offshore of the 700-m isobath just downstream of the bank. Velocities over the bank close to the coast are very weak (Figs. 2a and 3). South of the bank, southward velocities close to the coast increase, showing the spinup of a local coastal jet. In the "lee" of the bank between these two regions, the flow is nearly zero at the surface. At depth the flow is northward, establishing a recirculation area which may increase the retention of water parcels over the bank. Despite the highly idealized nature of the wind forcing and bottom topography used in this simulation, the results just described are qualitatively similar to observational results of flow around a shallow submarine bank (Heceta Bank) off the Oregon coast [see results from the Coastal Ocean Advance in Shelf Transport (COAST) program, e.g., Barth et al. (2005), Castelao and Barth (2005), Kosro (2005)]. The σ_θ cross-shelf sections (Fig. 3) indicate that upwelling is enhanced south of the bank. The mechanism responsible for this enhancement is the same as that described by Gan and Allen (2002a) for flow around a cape. The increased values of $\tilde{v}$ and decreased values of r near the bank change the cross-shelf momentum balance to a gradient wind (1), leading to additional ageostrophic decreases in the pressure near the bank. A negative along-shelf pressure gradient south of the bank is established, which is balanced by geostrophic onshore flow. The onshore flow helps advect denser water up the shelf, leading to enhanced upwelling there. The most downstream cross-section shown (Fig. 3) reveals that the flow at that location is very similar to the flow upstream of the bank and that the jet has reattached to the topography.

In the larger radius simulation, the offshore deflection of the jet is weak (Fig. 2b). The flow closely follows the topography and the export of cold water off the shelf at the surface is much less intense when compared with the smaller radius simulation. The 10°C isotherm continues to follow the 200-m isobath downstream of the bank. In this case, the flow in the "lee" of the bank

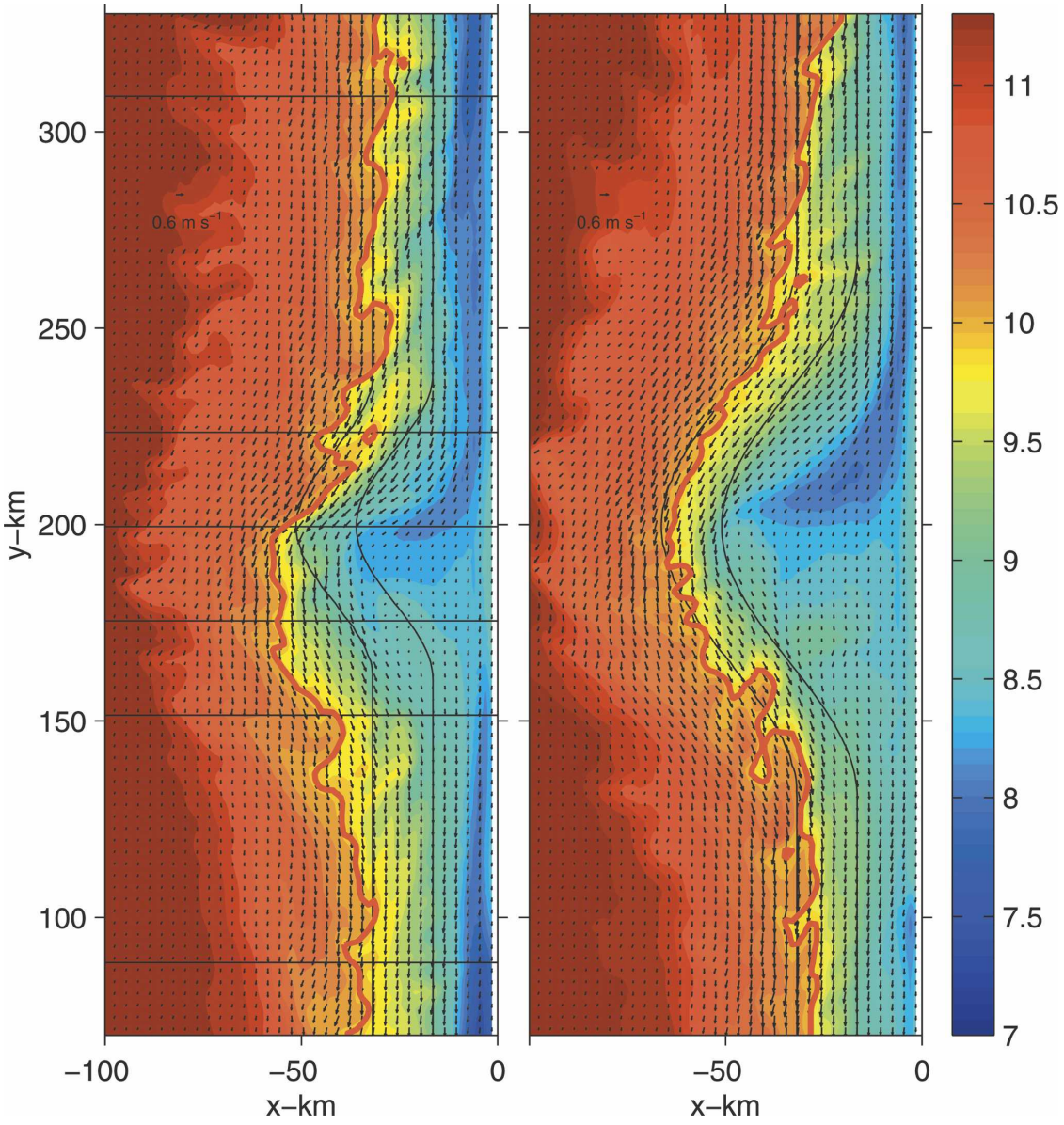

FIG. 2. Surface velocities and temperature (°C) at day 21 for simulations forced by moderate winds (0.125 Pa) and with Burger numbers equal to (a) 1.10 and (b) 0.38. The 100- and 200-m isobaths are shown. The thick red line is the 10°C isotherm. The thin lines in (a) mark the location of cross sections shown in Fig. 3.

is weak but still southward at all depths (not shown), and no recirculation region is established.

The depth-averaged cross-isobath flow for both simulations is shown in Fig. 4. Negative values indicate flow toward deeper water. As already inferred from the surface temperature field, the offshore-directed flow is strong in the Bu = 1.10 simulation, reaching almost 0.3 m s^{-1}. The cross-isobath transport (per meter along the isobath) at the 100-m isobath is 30 m^3 s^{-1}, much larger than the 1.2 m^3 s^{-1} cross-isobath transport in the surface Ekman layer. In the Bu = 0.38 simulation, the depth-averaged cross-isobath flow is weak, occupying a much smaller area, and rarely exceeds 0.1 m s^{-1}. These examples illustrate how significant a topographic feature can be for enhancing the off-shelf transport of material.

4. Parameter space analyses

This section explores the relative importance of wind forcing and bank geometry in causing the coastal upwelling jet to deflect offshore and cross isobaths. The model was run using upwelling-favorable winds with

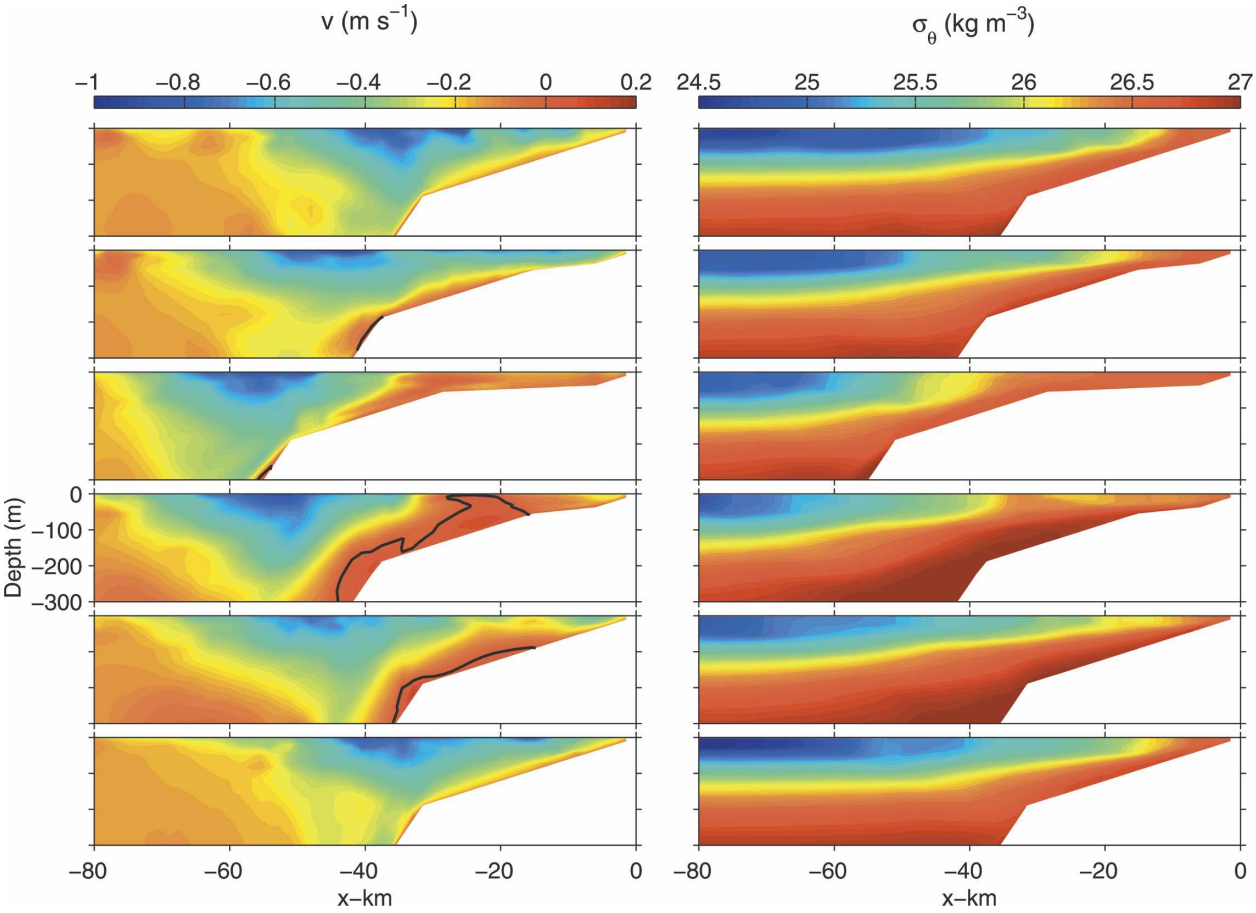

FIG. 3. Fields of (left) v and (right) σ_θ for cross-shelf sections at day 21 for simulation with Bu = 1.10. The black contour in the left panels is the zero v contour. Location of cross sections is shown in Fig. 2a.

eight different intensities (between 0.02 and 0.2 Pa), and using 11 different bottom topographies. The only difference between the topographies was the value of R. The other parameters affecting Ro and Bu (N and f) were kept constant. The relation between wind strength and Rossby number was approximately linear in the simulations. The estimated values of the amplitude of the separation (S_x) and of the downstream distance from the bank at which the maximum offshore displacement took place (S_y) on day 21, computed as defined in section 2, are shown in Figs. 5a and 5b. Results from earlier days are quantitatively similar except that the maximum Rossby numbers reached are smaller.

For low Ro, S_x is small, tending to increase as Ro increases. This is consistent with the idea that inertial effects play an important role in the separation process. Allen (2000) studied the conditions necessary for the flow in a homogeneous layer in contact with the topography to cross isobaths when topographic contours converge. The critical parameter (G) was the ratio of the final convergence of the contours and the minimum distance that can separate the two contours, while ensuring that the flow can remain strictly along the contours. If evaluated at the convergence, G was simply the square root of the reciprocal of the Rossby number if the flow follows the isobaths (Allen 2000). She found that under smaller G (larger Ro) the tendency to cross isobaths is larger. Allen (2000) did not consider any bending or curvature in the isobaths, as convergence effects were dominant in the area of interest in that study. Here topographic contours are parallel, and curvature effects dominate.

In addition to this general tendency of increasing S_x as Ro increases, there is significant variability in the response for different Burger numbers. For small Bu (bank radius considerably larger than the Rossby radius), S_x is relatively small, independent of the value of Ro. Most of the adjustment of the flow to the topography in that case happens in the northern part of the bank, and the along-shelf flow is nearly geostrophic to the south of the bank. The bank is large enough for the flow to adjust to the topographic variations, and the

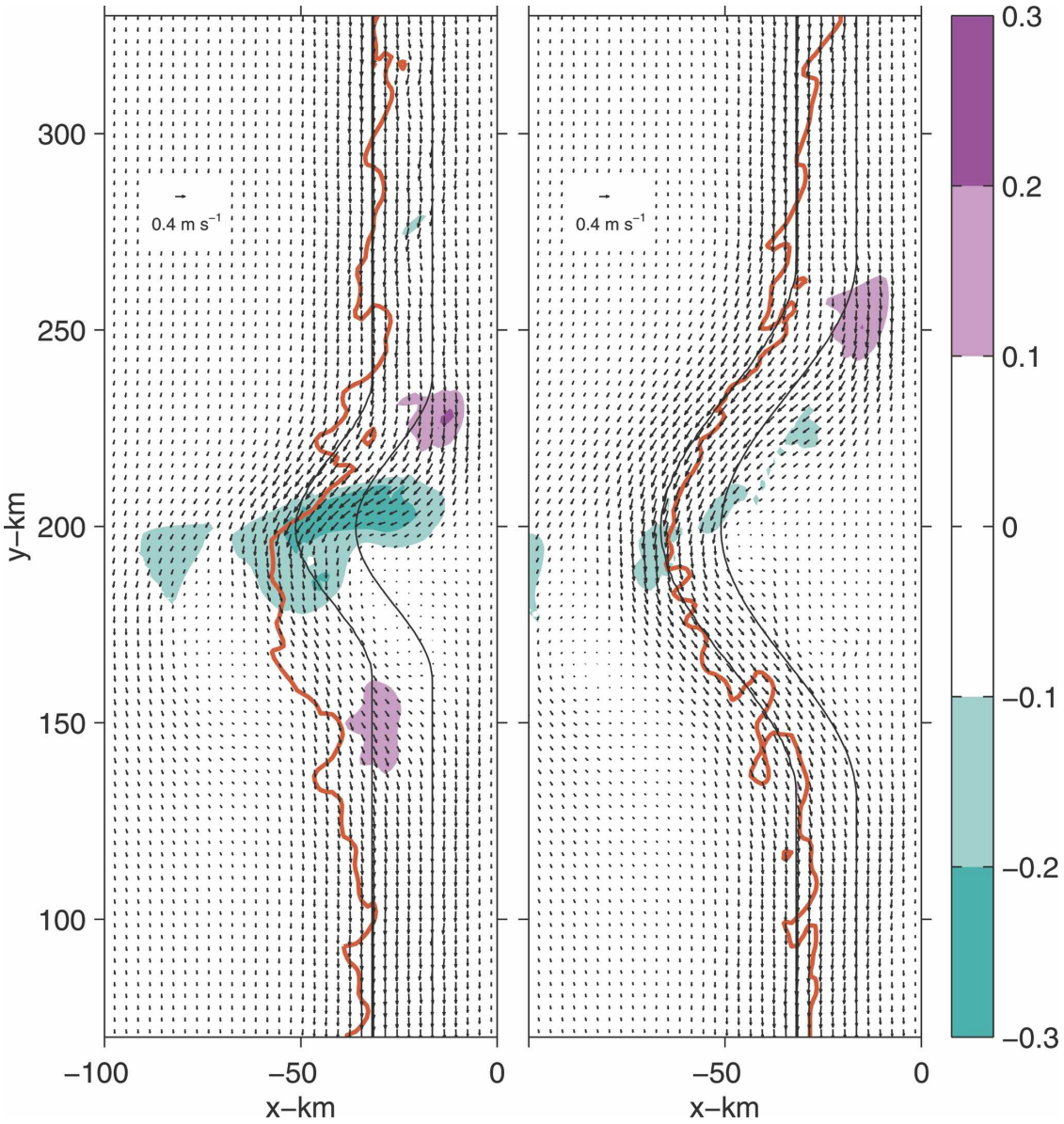

FIG. 4. Depth-averaged velocity vectors and cross-isobath depth-averaged velocity magnitudes (m s^{-1}, negative values indicate flow toward deeper water) at day 21 for simulations forced by moderate winds (0.125 Pa) and with Burger numbers equal to (a) 1.10 and (b) 0.38. The 100- and 200-m isobaths are shown. The thick red line is the 10°C isotherm at the surface.

offshore cross-isobath deflection experienced by the jet is small (see also Figs. 2b and 4b). For intermediate values of Ro (~0.2–0.25), an increase in Bu leads to an increase in the separation. For larger Ro, a maximum in S_x is found for Bu roughly between 0.7 and 1.5 (i.e., a bank with a radius roughly the same size of the internal Rossby radius). For Burger numbers larger than that, there is a decrease in S_x. As the topographic perturbation become considerably smaller than the deformation radius, it is "felt" less by the flow. This is a fundamental difference to Bormans and Garrett's (1989) study of buoyancy-driven flow around a corner. In their study, the angle between the walls upstream and downstream of the corner was 90°. A decrease in the radius of curvature of the wall led to the formation of a sharper corner, which enhanced separation and formation of a gyre downstream of the corner. Here the angle between the topographic contours upstream and downstream of the bank is zero. As the radius of curvature of the topography decreases below a critical value, it perturbs

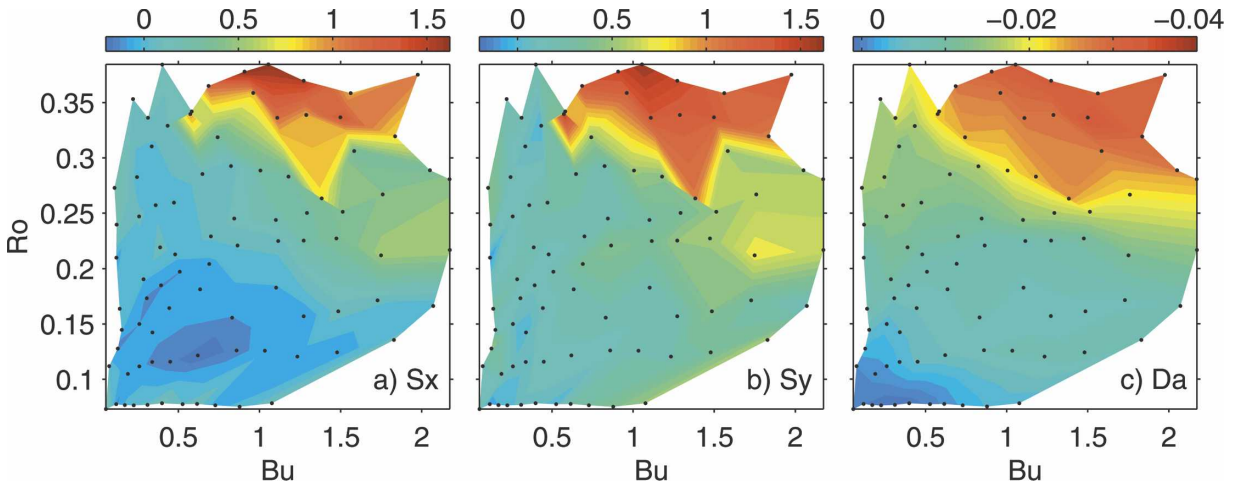

FIG. 5. (a) Offshore jet displacement (S_x), (b) downstream distance of maximum offshore displacement measured from midbank (S_y), and (c) cross-isobath depth-averaged flow averaged around the bank (D_a, m s^{-1}; see Fig. 1 for location) as a function of the Rossby number (Ro) and the Burger number (Bu) for numerical experiments indicated by black dots. See section 2 for definition of S_x, S_y, and D_a.

the flow less and less, leading to a decrease in S_x. Mysak and Tang (1974), using a linear, unforced, statistical perturbation theory for coastlines having small irregularities when compared with the radius of deformation, found that the correction to a Kelvin wave solution due to irregularities is $O(\varepsilon^2)$, where ε is the ratio of the typical scale of coastline irregularities and the radius of deformation. For small ε (large Bu), the correction is negligible. Despite the differences in the assumptions used in the studies, the present results are in qualitative agreement with their result.

The panel with the nondimensionalized downstream distance (S_y, Fig. 5b) shows a similar pattern. An increase in the Rossby number (jet more inertial) caused the location of maximum separation to move farther downstream. For small Burger numbers, S_y is small. As discussed above, the flow adjusts to the topography in the northern region of the bank, and the maximum offshore extent reached by the jet occurs close to midbank (S_y small). For some simulations with very low Bu, S_y is slightly negative, meaning that the maximum offshore extent reached by the jet occurred just upstream of the bank. As for S_x, S_y is maximum for Bu between 0.7 and 1.5 and large Ro.

The interaction of the flow with the topography leading to separation can substantially increase the transport of coastal water and the material it contains off the shelf into deeper waters (Fig. 4). The magnitude of the spatially averaged cross-isobath flow (D_a) is strongly dependent on both the bank geometry and wind forcing (Fig. 5c). Since it is closely related to the magnitude of the separation of the jet, the pattern of cross-isobath flow in parameter space is similar to the separation diagrams (Figs. 5a and 5b) with maximum offshore flow for large Rossby number and Burger numbers close to unity. The decrease in D_a for increasing Bu in the high Ro limit, however, is not as large as before. Also, D_a has a stronger dependence on *Ro* for low Bu than do S_x and S_y.

5. Dynamical analyses

To help to clarify the dynamical mechanisms involved in the flow adjustment to the topography, term balances in the depth-averaged along-shelf momentum equation are examined. That equation is written as

$$H^{-1}\left[\frac{\partial(VD)}{\partial t} + (\text{advection} - F^y) + fUD + \frac{D}{\rho_0}\frac{\partial P}{\partial y} - \frac{\tau_s^y}{\rho_0} + \frac{\tau_b^y}{\rho_0}\right] = 0, \quad (5)$$

where the terms in (5) are the tendency, nonlinear advection plus horizontal diffusion, Coriolis acceleration, pressure gradient, and surface and bottom stresses. In addition to the variables/parameters already defined, t is time, $D = H + \eta$ is the water depth, F^y is the horizontal diffusion term, P is pressure, and τ_s^y and τ_b^y are the along-shelf components of the surface and bottom stresses, respectively.

Terms in the depth-averaged along-shelf momentum equation (5) are shown in Fig. 6 for a simulation forced by moderate winds (Ro = 0.24) and with Bu = 1.10 (see also Figs. 2a and 3). Results from simulations with wind forcing of different magnitudes are qualitatively simi-

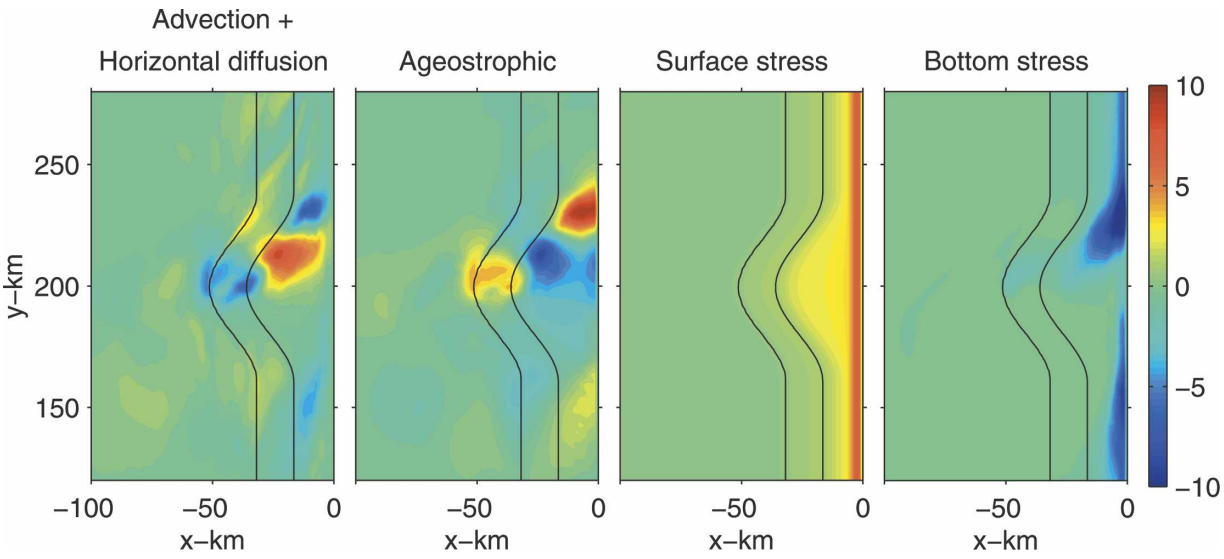

FIG. 6. Terms (m s^{-2}, multiplied by 10^6) from the depth-averaged along-shelf momentum Eq. (5) averaged around day 21 for simulation forced by moderate winds (0.125 Pa) and with Ro = 0.24, Bu = 1.10. The 100- and 200-m isobaths are shown.

lar. The largest terms in the vicinity of the bank are the Coriolis and the along-shelf pressure gradient. Those terms nearly balance each other, and the flow in the vicinity of the bank is geostrophic to lowest order. Since we are interested in departures from this balance, the two terms are only shown added together, representing the ageostrophic contribution to the balance. The tendency term is much smaller than the other terms everywhere in the domain, and therefore is not shown.

The primary balance in a narrow band close to the coast is between the surface and bottom stresses. The surface stress term decreases significantly offshore of the 35-m isobath, as does the bottom stress term away from the bank. Over the upstream half of the bank, the region of high bottom stress extends farther offshore, reaching the 60-m isobath. In the northern part of the bank close to the coast, the ageostrophic term is large and positive. This is the area where the jet first accelerates southward as it flows over shallower waters before turning offshore, as revealed by the negative nonlinear term. A large area over the bank is dominated by a negative ageostrophic term, which is balanced by positive advection in the upstream half of the bank. The negative ageostrophic term in the northern part of the bank is due to the negative Coriolis term overcoming the positive along-shelf pressure gradient; that is, there is an ageostrophic offshore flow over the bank. The positive advection term (both $U\partial V/\partial x$ and $V\partial V/\partial y$ are > 0) corresponds to the jet accelerating offshore. Offshore of that, the advection term is negative, as the flow accelerates back southward and is balanced by a positive ageostrophic term. At the southern half of the bank, the negative ageostrophic term is mostly balanced by the surface stress. There is yet another region where the advection term is negative just south of the bank. This indicates a local coastal jet is accelerated there, as confirmed by the surface velocity vectors shown in Fig. 2a. The nonlinear term is balanced by both the ageostrophic and the surface stress terms. In summary, the major balance in the along-shelf momentum equation over the bank is between the ageostrophic term and the nonlinear advection, with smaller contributions from the surface and bottom stresses.

The previous dynamical analysis suggests that the nonlinear terms play a major role in the offshore deflection of the jet. This is confirmed by comparing the previous results with results obtained from a simulation under the same conditions but using a linear version of the model. Without the inertial terms the flow closely follows the topographic contours (not shown). The cross-isobath flow is virtually nil, and the width of the upwelling region is constant with respect to the isobaths along the coast.

If the dynamics were linear, reversing the direction of wind would merely change the sign of all upwelling results (She and Klinck 2000). Simulations with the nonlinear model forced by downwelling-favorable winds produced substantially different results. The offshore deflection of the jet as it passes the bank is much weaker, and the depth-averaged cross-isobath flow is much reduced. This can be at least partially explained using a potential vorticity conservation argument. Consider a homogeneous fluid flowing over a submarine bank forced by upwelling-favorable winds. In that sce-

nario, a water particle turns anticyclonically ($\zeta < 0$, where ζ is the relative vorticity) as it reaches the shallow waters over the bank (water column is squashed) in order to converse potential vorticity $[(f + \zeta)/H]$. The particle is then displaced offshore toward deeper isobaths, favoring separation. In the downwelling-favorable wind scenario, the anticyclonic vorticity acquired by the water particle as it moves over shallow waters (i.e., as it flows over the bank and the water column is squashed) forces it to remain close to the coast, inhibiting separation. Using realistic stratification, as in the present case, will decrease but not eliminate this constraint on the flow. A detailed analysis of the differences in the flow response to upwelling- and downwelling-favorable winds over a submarine bank is underway (M. Whitney and J. Allen 2005, personal communication).

Term balances in Eq. (5) for the nonlinear version of the model considering the same wind forcing as before but with a bank with a much larger radius of curvature (Bu = 0.38, as in Fig. 2b, not shown) show most of the features described above in Fig. 6, but the flow adjustment to the topography is concentrated in the northern part of the bank. In the smaller radius simulation (Bu = 1.10, Fig. 6), the topographic contours turn onshore just downstream of the area in which the jet moved offshore (area of positive advective terms). For the large bank simulation, the shelf continues to widen downstream of the area where the jet moves offshore, resulting only in weak cross-isobath deflection of the upwelling jet (Fig. 4b).

6. Asymmetry in the bank geometry

Results shown so far used a bank with symmetric geometry; that is, the bottom topography on the downstream half of the bank mirrors the topography on the upstream half. This is often not the case in the ocean. One example of an asymmetric bank can be found off the Oregon coast. The Heceta Bank complex is characterized by a slowly widening shelf in the upstream region of the bank with a relatively sharp transition toward a narrow shelf downstream of the bank. To investigate the importance of bank asymmetry in driving the coastal upwelling jet toward deeper waters, a bottom topography with two different radii of curvature was used (Fig. 7a). On the upstream half of the bank, R is large when compared with the internal Rossby radius. In this situation, separation is strongly inhibited (Figs. 5a–c). The downstream half of the bank is characterized by a much smaller radius of curvature. Note that the curving isobaths with different radii are not concentric in order to make the topography continuous. The geometry is chosen so as to approximately represent the 200-m isobath at Heceta Bank. The upstream radius used is probably underestimated for Heceta Bank, as the region of the widening shelf extends farther north than represented in the model. A larger upstream bank radius was not used owing to the limited size of the domain. A symmetric topography is also considered, with a radius of curvature equal to the larger radius considered in the asymmetric case. Comparing the results from the two cases allows the importance of bank asymmetry on flow response to be analyzed. The model is forced by moderate winds (0.125 Pa) in both simulations.

In the symmetric case (Fig. 7b) the jet follows the topography as expected, resulting in no significant cross-isobath deflection of the 9°C isotherm. In the asymmetric simulation, the jet inertially overshoots the topography south of the bank (Fig. 7c). Note that this is different from the jet separation discussed in the previous sections. Before, when the same wind forcing and symmetric topographies were used, separation occurred for an ideal range of bank sizes (those that make Bu close to 1). Here, the upstream radius of curvature of the topography is large (making Bu small) and separation should be inhibited. This indeed is the case, as seen in Fig. 7b. The strong cross-isobath flow observed in the downstream half of the asymmetric bank occurs because of the sharp bend in topography contours there (Fig. 7c), and not the bank radius falling in an ideal range. A third topography was also used, characterized by a less sharp bend in the contours at the downstream part of the bank (intermediary between symmetric and asymmetric topographies shown in Figs. 7b and 7c, not shown). The distance measured from the coast reached by the 9°C isotherm at the surface is roughly the same in all three cases. Although the offshore deflection experienced by a water particle is roughly the same in all cases, cold waters reach much deeper waters in the asymmetric case (Fig. 7c). The jet advects upwelled water southward, forming a small tongue of cold water just downstream of the bank, as seen by the bend in the 9°C contour.

The importance of the topographic asymmetry is further illustrated by comparing the depth-averaged velocity magnitudes along the cross sections marked in Figs. 7b and 7c. The magnitudes of the depth-averaged velocities along the downstream cross sections in the two topographies are different owing to the depth profiles being different. For ease of comparison, velocities for each case are normalized by their maximum values (Fig. 7d). In both cases, the jet lies over the 190-m isobath upstream of the bank. In the symmetric case, maximum velocities are still located at the shelf break

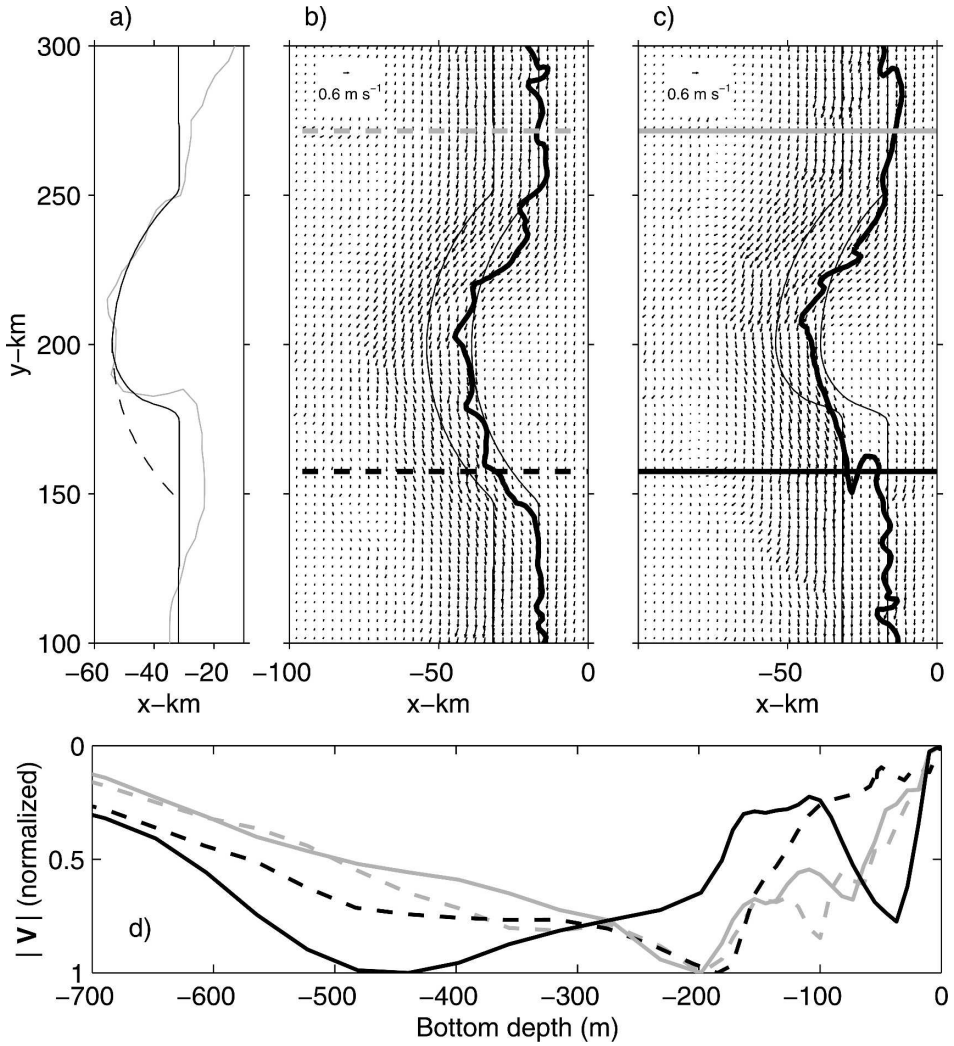

FIG. 7. (a) Model topography. The gray line is the 200-m isobath at Heceta Bank. Dashed (solid) line is the 200-m isobath for symmetric (asymmetric) topography. Remaining top panels show surface velocities at day 21 for simulations forced by moderate winds (0.125 Pa) and with (b) symmetric and (c) asymmetric bottom topography. The 100- and 200-m isobaths are shown. The thick black contour is the 9°C isotherm. (d) Normalized depth-averaged velocity magnitudes along cross sections in (b) and (c) as a function of bottom depth. Dashed (solid) line is for symmetric (asymmetric) topography. Gray (black) line is for the cross sections located upstream (downstream) of the bank.

along the 190-m isobath at the downstream section. Inshore of the 150-m isobath velocities are weaker than in the upstream cross-shelf section, as the region over the bank close to the coast is characterized by weak velocities. In the asymmetric case, on the other hand, the jet lies over the 450-m isobath. Note again that the location of the velocity maxima in both topographies along the downstream section would be roughly coincident if the cross-section profiles were plotted against distance measured from the coast instead of against bottom depth. This happens because most of the adjustment of the flow to the topography perturbation occurs on the upstream half of the bank (see Fig. 6) where the topography in the two cases is identical. In the asymmetric case, a local coastal jet is spun up inshore of the separated jet (similar to spinup discussed in Fig. 6).

These results suggest that for an asymmetric bank, which cannot be fully characterized by a single radius of curvature, the upstream radius of curvature dominates in terms of causing the jet to deflect offshore. The large upstream bank radius used does not generate jet separation. The asymmetry in the downstream half of the bank, on the other hand, can enhance the cross-isobath transport of upwelled waters off the shelf. This is in

agreement with observations from the 2001 upwelling season off Oregon, which showed large amounts of cold, upwelled water (with high chlorophyll fluorescence) being flushed off Heceta Bank toward deeper waters at the downstream asymmetry (Castelao and Barth 2005).

7. Application to Heceta Bank

The idealized topography used in the last section was chosen to fit the 200-m isobath around Heceta Bank because it could clearly illustrate the effect of an asymmetric topography in the flow response. Over Heceta Bank, however, the radius of curvature is also dependent on the isobath. Using surface velocity data from land-based coastal radar, Kosro (2005) showed that there is a tendency for the primary equatorward jet just upstream of Heceta Bank to be centered near the 80-m isobath. The asymmetry in the 80-m isobath is much reduced relative to the 200-m isobath. In fact, the 80-m isobath in the Heceta Bank region can be approximated by a symmetric topography with $R = 15$ km after an 8° anticlockwise axes rotation (Fig. 8; this is the average current direction upstream of the bank; Kosro 2005). Using the averaged temperature and salinity profiles from spring and summer 2001 (Castelao and Barth 2005), we obtain Bu = 1.09 and 0.7, respectively. Rossby number estimates upstream of Cape Foulweather (see Fig. 8 for location) using surface currents measured with land-based, high-frequency radar during strong wind forcing are in excess of 0.3. In this range, the coastal jet following the 80-m isobath could separate from the topography (Fig. 5). A qualitative comparison using surface currents measured with the coastal radar confirms this. The average offshore location of the jet changes near Cape Foulweather, where the shelf starts to widen around Stonewall and Heceta Banks, and surface velocities are deflected offshore (Kosro 2005). For strong equatorward wind stress (high Rossby number), there is significant flow across the 80-m isobath over the bank (see Fig. 13a from Kosro 2005).

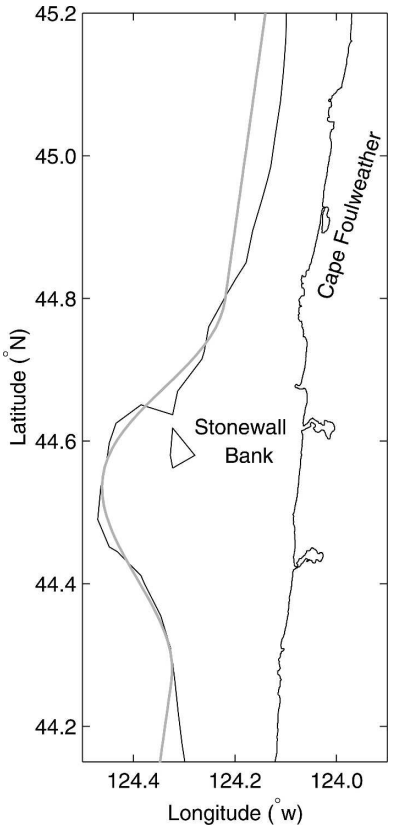

FIG. 8. Coastline and 80-m isobath at the Heceta Bank region. The gray line is a symmetric idealized bank with $R = 15$ km after axes were rotated anticlockwise by 8°.

8. Summary and conclusions

The majority of studies to date of flow over topography exploring a wide range in parameter space considered either a homogeneous or a density-driven flow. Studies of stratified, wind-forced flow over topography, on the other hand, generally did not span a large region in parameter space. Here, a high-resolution numerical ocean circulation model is used to study the effects of a shallow submarine bank on stratified flow forced by surface wind stress. Many numerical experiments were run, differing in the magnitude of the forcing and on the geometric characteristics of the bank, such that variations in the Rossby number and the Burger number are large between experiments.

The model results away from the bank, that is, in the area of straight topographic contours, are consistent with two-dimensional coastal upwelling, with isopycnals tilting upward toward the coast and the development of a vertically sheared coastal upwelling jet. The circulation over the bank is much more complicated; for some bank geometries and wind forcing the coastal jet separates from the topography and is found over much deeper waters downstream of the bank than upstream of it. In those cases, a local coastal jet is generally spun up close to the coast, inshore of the separated jet. For other topographies and wind forcing, the jet follows the topographic contours.

Analysis of various measures of the jet separation as a function of the Rossby number and of the Burger number showed that the flow response to the topography perturbation is strongly dependent on both parameters. For a given bank geometry, an increase in the wind forcing generally leads to an increase in the off-

shore deflection experienced by the jet downstream of the bank, enhancing cross-isobath transport. This is particularly true for simulations with Burger number close to unity. This suggests inertia is important in driving the cross-isobath flow, which is confirmed by both looking at term balances in the depth-averaged alongshelf momentum equation and by comparing with results from a linear version of the model. That was not the case for low Burger number simulations, where there is little jet separation independent of the Rossby number. In that case, the adjustment of the flow to the topography occurs in the northern region of the bank. The shelf width continues to increase to the south of that location for low Burger number simulations, resulting in weak cross-isobath deflection of the jet. A decrease in the jet separation for high Ro was also found in the limit of large Burger number (when compared with simulations with Bu $\sim$1) since the bank in that case acts only as a small perturbation to the flow. In summary, maximum separation and cross-isobath transport is found for high Rossby number and for banks with a radius of curvature similar to the internal deformation radius. For the Heceta Bank region off Oregon, Bu $\sim$1 during spring and summer, and Ro is large for moderate to strong wind forcing, aiding separation.

We also investigated the importance of an asymmetry in the bank geometry on the cross-isobath deflection of the jet, as many oceanic submarine banks are not symmetric. The asymmetric geometry is characterized by a slowly widening shelf in the upstream part of the bank and a sharp transition toward a narrow shelf in the downstream half of the bank. Results show that the upstream radius of curvature is dominant in terms of causing offshore deflection of the jet. The geometric asymmetry, on the other hand, with the sharp onshore bend in the topography contours at the downstream part of the bank, can cause the jet to cross isobaths, significantly increasing the off-shelf transport.

Last, we point out that the wind stress was considered spatially homogeneous in all simulations in order to reduce the span of the parameter space. Spatially variability in the wind may contribute to jet separation. Samelson et al. (2002) suggested that the coastal jet separation near Cape Blanco, Oregon, might be controlled by enhanced local wind forcing in the vicinity of the cape. The effect of spatial variability in the forcing, including cross-shore variations (i.e., the wind stress curl), on the separation of a coastal jet is a subject for future research.

Acknowledgments. The authors are grateful to J. Allen and M. Whitney for helpful comments and suggestions; P. M. Kosro kindly provided the land-based, high-frequency radar data used for estimating the Rossby number upstream of Heceta Bank. This research was supported by the National Science Foundation under Grant OCE-9907854. Author RC was supported by the Brazilian National Research Council (CNPq Grant 200147/01-3) and by the Inter American Institute for Global Change Research (IAI), through project SACC (CRN-061). We dedicate this paper to the memory of Dr. David C. Chapman, for this is just the type of coastal geophysical fluid dynamics problem that he loved to explore.

REFERENCES

Allen, J. S., P. A. Newberger, and J. Federiuk, 1995: Upwelling circulation on the Oregon continental shelf. Part I: Response to idealized forcing. *J. Phys. Oceanogr.,* **25,** 1843–1866.

Allen, S. E., 2000: On subinertial flow in submarine canyons: Effect of geometry. *J. Geophys. Res.,* **105,** 1285–1297.

Arthur, R. S., 1965: On the calculation of vertical motion in eastern boundary currents from determinations of horizontal motion. *J. Geophys. Res.,* **70,** 2799–2803.

Barth, J. A., S. D. Pierce, and R. L. Smith, 2000: A separating coastal upwelling jet at Cape Blanco, Oregon and its connection to the California Current system. *Deep-Sea Res. II,* **47,** 783–810.

——, ——, and R. M. Castelao, 2005: Time-dependent, wind-driven flow over a shallow midshelf submarine bank. *J. Geophys. Res.,* **110,** C10S05, doi:10.1029/2004JC002761.

Blumberg, A. F., and G. L. Mellor, 1987: A description of a three-dimensional coastal ocean circulation model. *Three-Dimensional Coastal Ocean Models,* N. Heaps, Ed., Coastal and Estuarine Sciences, Vol. 4, Amer. Geophys. Union, 1–16.

Bormans, M., and C. Garrett, 1989: A simple criterion for gyre formation by the surface outflow from a strait, with application to the Alborean Sea. *J. Geophys. Res.,* **96,** 12 637–12 644.

Boyer, D. L., and L. Tao, 1987: On the motion of linearly stratified rotating fluids past capes. *J. Fluid Mech.,* **180,** 429–449.

Brink, K. H., 1983: The near-surface dynamics of coastal upwelling. *Progress in Oceanography,* Vol. 12, Pergamon, 223–257.

Camerlengo, A. L., and J. J. O'Brien, 1980: Open boundary conditions in rotating fluids. *J. Comput. Phys.,* **35,** 12–35.

Castelao, R. M., and J. A. Barth, 2005: Coastal ocean response to summer upwelling favorable winds in a region of alongshore bottom topography variations off Oregon. *J. Geophys. Res.,* **110,** C10S04, doi:10.1029/2004JC002409.

Clarke, A. J., 1977: Wind-forced linear and nonlinear Kelvin waves along an irregular coastline. *J. Fluid Mech.,* **83,** 337–348.

Dale, A. C., and J. A. Barth, 2001: The hydraulics of an evolving upwelling jet flowing around a cape. *J. Phys. Oceanogr.,* **31,** 226–243.

Gan, J., and J. S. Allen, 2002a: A modeling study of shelf circulation off northern California in the region of the Coastal Ocean Dynamics Experiment: Response to relaxation of upwelling winds. *J. Geophys. Res.,* **107,** 3123, doi:10.1029/2000JC000768.

——, and ——, 2002b: A modeling study of shelf circulation off northern California in the region of the Coastal Ocean Dy-

namics Experiment 2. Simulations and comparisons with observations. *J. Geophys. Res.,* **107,** 3184, doi:10.1029/2001JC001190.

Haidvogel, D. B., A. Beckman, and K. Hedstrom, 1991: Dynamical simulation of filament formation and evolution in the coastal transition zone. *J. Geophys. Res.,* **96,** 15 017–15 040.

Holton, J. R., 1992: *An Introduction to Dynamic Meteorology.* Academic Press, 511 pp.

Huyer, A., 1983: Coastal upwelling in the California Current system. *Progress in Oceanography*, Vol. 12, Pergamon, 259–284.

Kosro, P. M., 2005: On the spatial structure of coastal circulation off Newport, Oregon, during spring and summer 2001 in a region of varying shelf width. *J. Geophys. Res.,* **110,** C10S06, doi:10.1029/2004JC002769.

Kundu, P. K., J. S. Allen, and R. L. Smith, 1975: Modal decomposition of the velocity field near the Oregon coast. *J. Phys. Oceanogr.,* **5,** 683–704.

McCreary, J. P., Y. Fukamachi, and P. K. Kundu, 1991: A numerical investigation of jets and eddies near an eastern ocean boundary. *J. Geophys. Res.,* **96,** 2525–2534.

Mellor, G. L., and T. Yamada, 1982: Development of a turbulence closure model for geophysical fluid problems. *Rev. Geophys.,* **20,** 851–875.

Mysak, L. A., and C. L. Tang, 1974: Kelvin wave propagation along an irregular coastline. *J. Fluid Mech.,* **64,** 241–261.

Narimousa, S., and T. Maxworthy, 1989: Application of a laboratory model to the interpretation of satellite and field observations of coastal upwelling. *Dyn. Atmos. Oceans,* **13,** 1–46.

Oke, P. R., and Coauthors, 2002a: A modeling study of the three-dimensional continental shelf circulation off Oregon. Part I: Model–data comparisons. *J. Phys. Oceanogr.,* **32,** 1360–1382.

——, J. S. Allen, R. N. Miller, and G. D. Egbert, 2002b: A modeling study of the three-dimensional continental shelf circulation off Oregon. Part II: Dynamical analysis. *J. Phys. Oceanogr.,* **32,** 1383–1403.

Peffley, M. B., and J. J. O'Brien, 1976: A three-dimensional simulation of coastal upwelling off Oregon. *J. Phys. Oceanogr.,* **6,** 164–180.

Samelson, R., and Coauthors, 2002: Wind stress forcing of the Oregon coastal ocean during the 1999 upwelling season. *J. Geophys. Res.,* **107,** 3034, doi:10.1029/2001JC000900.

She, J., and J. M. Klinck, 2000: Flow near submarine canyons driven by constant winds. *J. Geophys. Res.,* **105,** 28 671–28 694.

Smagorinsky, J., 1963: General circulation experiments with primitive equations. I. The basic experiment. *Mon. Wea. Rev.,* **91,** 99–164.

Yoshida, K., 1967: Circulation in eastern tropical oceans with special references to upwelling and undercurrents. *Japanese J. Geophys.,* **4,** 4–75.